Materials Reliability Program Elastic-Plastic Finite Analysis: Single and Double-J Hot Leg Nozzle-to-Pipe Welds (MRP-33)

Welding Residual and Operating Stresses

Technical Report

Materials Reliability Program Elastic-Plastic Finite Analysis: Single and Double-J Hot Leg Nozzle-to-Pipe Welds (MRP-33)

Welding Residual and Operating Stresses

1001501

Final Report, April 2002

EPRI Project Manager
A. McIlree

EPRI • 3412 Hillview Avenue, Palo Alto, California 94304 • PO Box 10412, Palo Alto, California 94303 • USA
800.313.3774 • 650.855.2121 • askepri@epri.com • www.epri.com

ORGANIZATION(S) THAT PREPARED THIS DOCUMENT

Dominion Engineering, Inc.

ORDERING INFORMATION

Requests for copies of this report should be directed to EPRI Orders and Conferences, 1355 Willow Way, Suite 278, Concord, CA 94520, (800) 313-3774, press 2 or internally x5379, (925) 609-9169, (925) 609-1310 (fax).

CITATIONS

This report was prepared by

Dominion Engineering, Inc.
6862 Elm Street
McLean, Virginia 22101

Principal Investigators
S. Hunt
D. Gross
M. Fleming

This report describes research sponsored by EPRI.

The report is a corporate document that should be cited in the literature in the following manner:

Materials Reliability Program Elastic-Plastic Finite Analysis: Single and Double-J Hot Leg Nozzle-to-Pipe Welds (MRP-33): Welding Residual and Operating Stresses, EPRI, Palo Alto, CA: 2002. 1001501.

REPORT SUMMARY

This report documents an elastic-plastic finite analysis of cracking in idealized single-J and double-J hot leg nozzle-to-pipe welds similar to those at Ringhals 4 and VC Summer.

Background

Primary water stress corrosion cracking (PWSCC) of Alloy 600 nozzles and penetrations in pressurized water reactor (PWR) plant primary system pressure boundaries has been a recurring problem since the mid 1980s. During the second half of 2000, cracks were discovered in Alloy 82/182 welds joining carbon steel reactor vessel hot leg nozzles to stainless steel pipes at Ringhals 4 and VC Summer. Both cases involved axial cracks in the weld metal. In the case of VC Summer, one axial crack appeared to have initiated at a weld repair location and then developed into a leak that deposited over 200 pounds of boric acid crystals outside the pipe near the weld. At VC Summer, a short circumferential crack also was discovered on the inside diameter (ID) region of the Alloy 182 weld clad. This circumferential crack arrested when it reached the carbon steel base material.

The root-cause analyses performed by the utility and contractor attributed the cracking to PWSCC of the Alloy 82/182 weld caused by the combination of susceptible material, high-tensile stresses, and the primary water environment.

Objectives

- To determine welding residual and operating condition stresses in idealized single-J and double-J weld joints similar to those at VC Summer and Ringhals—including the effect of reported weld repairs at VC Summer— using elastic-plastic finite element analyses.

- To demonstrate—for information purposes only—the role of differential thermal expansion between carbon and stainless steel materials in bimetallic joints by including an idealized bimetallic joint in the analyses.

Approach

The project team performed elastic-plastic finite element analyses to determine welding residual and operating condition stresses in idealized single-J and double-J weld joints similar to those at VC Summer and Ringhals, including the effect of reported weld repairs at VC Summer. Since information was limited on details of the original fabrication and weld repairs at VC Summer, three different cases were analyzed: (1) the as-designed weld configuration, (2) an as-repaired case with outside diameter (OD) repair weld passes made first and ID repair passes last, and (3) an as-repaired case with ID repair welds made first and OD welds last. Similarly, for the double-J weld configuration, the team considered two different cases: one with the OD side welded first and one with the ID side welded first.

The project team also performed analyses of an idealized bimetallic pipe joint between carbon steel and stainless steel. This elastic analysis case is included for information purposes to demonstrate the role of differential thermal expansion between carbon and stainless steel materials in bimetallic joints.

Results

All cases analyzed for both the single-J and double-J weld show that hoop stresses exceed axial stresses along the ID surface, indicating that cracks—should they initiate at the inside surface of the welds—would be axially oriented.

Analyses of both the single-J weld and double-J weld configurations show that welds made first at the OD and completed at the ID have higher hoop stresses along the ID surface than welds completed at the OD.

With the exception of the as-repaired single-J case welded at the ID first, there are relatively high-tensile operating condition hoop stresses of 41-53 ksi on the inside surface of the weld and buttering. Addition of new passes on the outside of the weld does not create sufficient inward deflection of the pipe to change the stress in initial passes from tensile to compressive.

In all cases analyzed, there are relatively high hoop stresses through the weld thickness, indicating the potential for deep cracks to be axially oriented. Through-thickness axial stresses are significantly less and approach zero in some regions.

EPRI Perspective

This work provides insight into the influence of welds and OD and/or ID weld repairs on the residual stresses in RV piping welds. The modeling work did not attempt to replicate the complex sequence of repairs thought to have been performed at VC Summer. Rather, the intent was simply to develop an appreciation of the magnitude and direction of the stresses that could be developed in a VC Summer–type single J-groove weld and a Ringhals-type double J-groove weld preparation. The finite element analysis results were extremely fruitful in demonstrating that hoop stresses, which lead to axial cracks, were dominant in the weld metal. Results also demonstrated that a small region of axial stress exists on the ID surface of the weld buttering at the location where a circumferential crack was observed in the VC Summer destructive examination.

Keywords

Welding residual stresses
Finite element analysis
PWSCC of alloy 600 weld metals
SCC of alloys 82 and 182
Reactor vessel nozzles

ABSTRACT

Primary Water Stress Corrosion Cracking (PWSCC) in reactor pressure vessel nozzle to pipe welds was observed at VC Summer and at Ringhals 4 during the second half of 2000. Following the discovery of leakage at VC Summer, EPRI sponsored elastic-plastic finite element analyses of the VC Summer single-J groove and Ringhals 4 double J-groove nozzle weld configurations to assess the operating condition stresses in the welds. An assessment of the stress distributions in these welds provides insight regarding the likely orientation of cracks in the nozzle welds should cracks initiate.

CONTENTS

LIST OF FIGURES

LIST OF TABLES

1 INTRODUCTION

Primary Water Stress Corrosion Cracking (PWSCC) of Alloy 600 nozzles and penetrations in PWR plant primary system pressure boundaries has been a recurring problem since the mid 1980's. During the second half of 2000, cracks were discovered in Alloy 82/182 welds joining low-alloy steel reactor vessel hot leg nozzles to stainless steel pipes at Ringhals 4 and VC Summer. Both cases involved axial cracks in the Alloy 82/182 weld metal, and in the case of VC Summer, one of the axial cracks developed into a leak that resulted in over 200 pounds of boric acid crystals being deposited outside the pipe near the weld. In the case of VC Summer, a short circumferential crack was also discovered in a region of Alloy 182 weld clad. This circumferential crack arrested when it reached the carbon steel base material.

The root cause analyses performed by the utilities and contractors attributed the cracking to PWSCC of the Alloy 82/182 weld caused by the combination of susceptible material, high tensile stresses and the primary water environment. Weld repairs were identified as a potential contributing factor at VC Summer.

The purpose of this document is to describe elastic-plastic finite element analyses to determine the welding residual and operating condition stresses in idealized single-J and double-J weld joints similar to those at VC Summer and Ringhals 4, including the effect of reported weld repairs at VC Summer.

Analyses are also included for the case of an idealized bimetallic pipe joint with low-alloy steel on one side and stainless steel on the other side. This elastic analysis case is included for information purposes to demonstrate the role of differential thermal expansion between carbon and stainless steel materials in bimetallic joints.

2 GEOMETRIES AND MATERIALS ANALYZED

The purpose of this section is to describe the pipe and weld geometry and the materials that were analyzed. This includes a description of the assumed repairs for the case of the single-J weld.

2.1 Idealized Bimetallic Pipe Joint

A model of an idealized bimetallic pipe joint with low-alloy steel material on one side and stainless steel material on the other was analyzed as part of the current study. The pipe inside and outside diameters and the materials are the same as reported for the single-J welded pipe.

The nozzle and pipe materials used were as reported by EPRI for the single-J weld nozzle:

- SA 508 Class 2 low-alloy steel[1]
- Type 304 stainless steel pipe[2]

– Results of the idealized model analysis are presented in Section 4.1.

2.2 Single-J Hot Leg Nozzle to Pipe Weld

The second finite element model, shown in Figure 2-1, represents a single-J weld similar to that at VC Summer. The pipe inside diameter and wall thickness were reported to be 29" and 2.33", respectively. The cladding thickness was reported to be 0.193" (1).

Materials were reported by EPRI to be:

- SA 508 Class 2 low-alloy steel
- Type 304 stainless steel pipe
- Alloy 82/182 weld and buttering
- Type 309 stainless steel cladding

1 This material is referred to as "SA 508 Grade 2 Class 1" material in the 1998 ASME Boiler and Pressure Vessel Code.

2 SA 376 304N stainless steel pipe material was included in the finite element model.

Several repairs are reported to have been made during welding of the VC Summer Hot Leg “A” nozzle. The sequence is described in a series of drawings by Duke Engineering and Services dated November 14, 2000 (1). At the angular position of the through-wall axial crack, the following sequence is described:

– The weld was deposited to a depth of 0.7" from the inside surface of the pipe.

– The weld was ground out from the outside to the root level and then rewelded to 0.85".

– The weld was back gouged from the inside surface of the pipe to a depth of 0.38-0.5" from the inside surface and the back gouged area rewelded.

– Welding then continued from the outside to a total depth of about 1.5" measured from the inside.

– At this point, the weld was repaired again from both the inside and outside. Since it is not known which was performed first, both options were evaluated.

– The ID repair was assumed identical to the previous ID repair.

– The OD repair was assumed to involve only minor grinding followed by filling the remainder of the weld to the outside surface of the pipe.

Since there is significant uncertainty regarding the exact repair sequence, it was determined that more sophisticated 3D type modeling is not warranted. The 2D axisymmetric modeling is expected to provide most of the useful information that would be obtained from a more detailed 3D model.

2.3 Double-J Hot Leg Nozzle to Pipe Weld

The third model, shown in Figure 2-2, represents a double-J weld similar to that at Ringhals 4. Selected dimensions for this model were provided by EPRI. In order to compare analysis results for the two designs on an equal basis, the pipe inside and outside diameters were assumed to be the same as for the single-J geometry. Dimensions not explicitly provided were scaled from the EPRI drawing.

The materials for the double-J nozzle are assumed to be the same as for the idealized bimetallic pipe and single-J nozzle:

– SA 508 Class 2 low-alloy steel

– Type 304 stainless steel pipe

– Alloy 82/182 weld and buttering

– Type 309 stainless steel pipe cladding

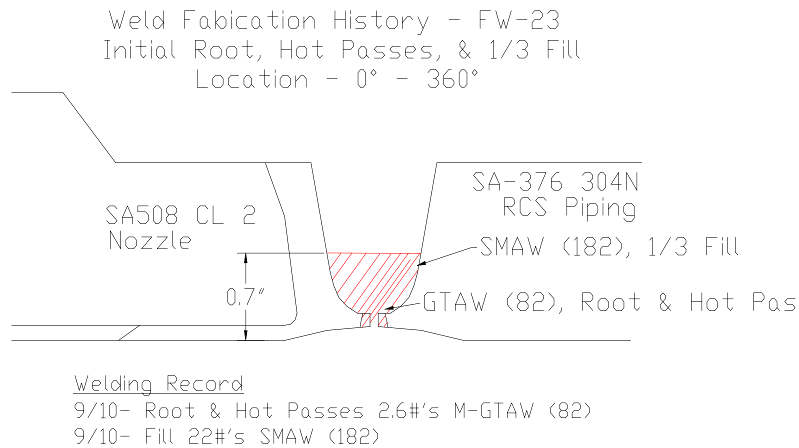

Figure 2-1a. Weld Geometry and Materials

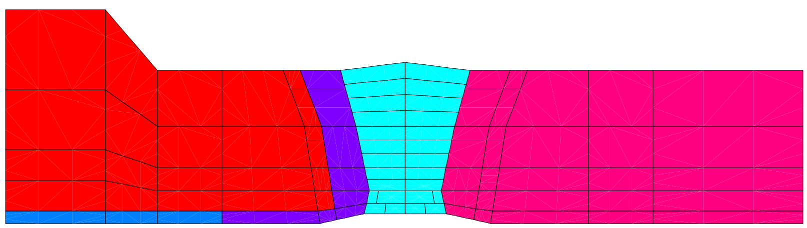

Figure 2-1b. Finite Element Model — Element Plot

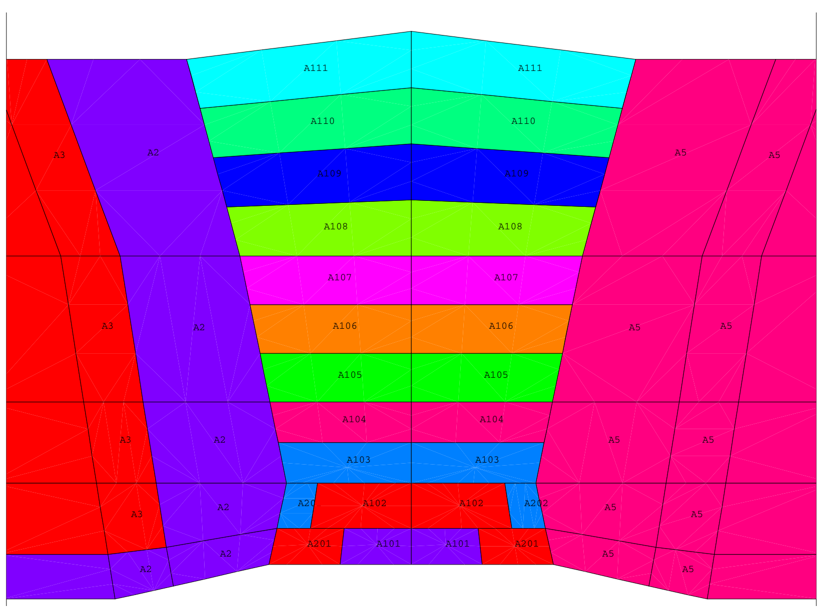

Figure 2-1c. Finite Element Model — Weld Areas

Figure 2-1
Nozzle and Weld Geometry – Single-J Groove Weld

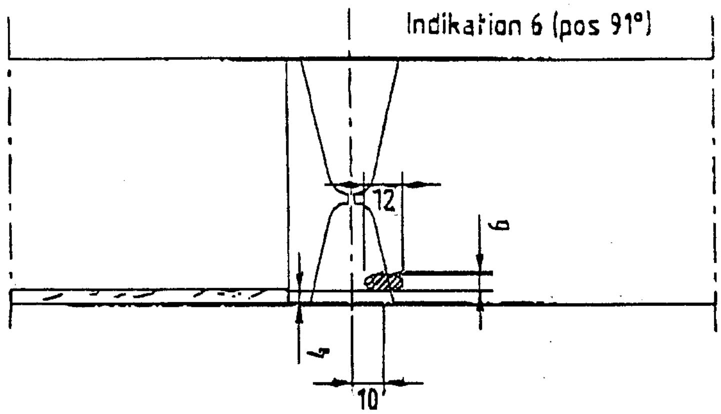

Figure 2-2a. Weld Geometry

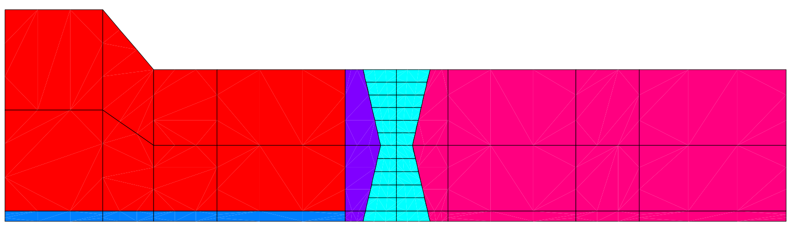

Figure 2-2b. Finite Element Model — Element Plot

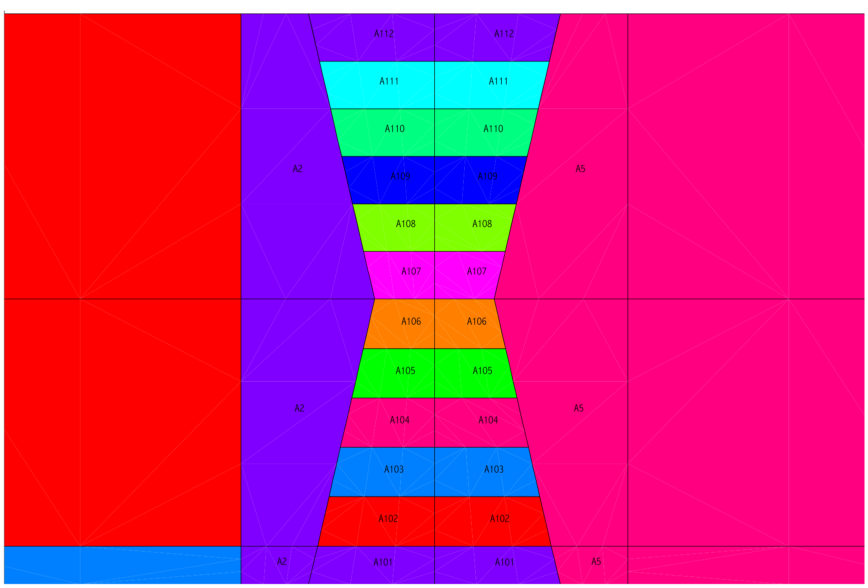

Figure 2-2c. Finite Element Model — Weld Areas

Figure 2-2
Nozzle and Weld Geometry – Double-J Groove Weld

3
ANALYSIS METHOD

The following is a brief description of the analysis method used for the three models.

3.1 Finite Element Program

Finite element analyses were performed using Revision 5.6 of the ANSYS general-purpose finite element computer program. The analyses were performed on a Hewlett-Packard B2000 workstation.

3.2 Geometric Models

All nozzle configurations/cases were analyzed using axisymmetric models. The model of the idealized bimetallic pipe joint consists of lengths of low-alloy steel and stainless steel pipe (no weld metal is included). The single-J and double-J nozzle-to-pipe weld models consist of a short length of the low-alloy steel nozzle, stainless steel cladding on the inside of the nozzle, Alloy 182 buttering, stainless steel pipe, and the Alloy 82/182 weld.

All elements are four-node quadrilateral elements. A large number of four-node elements is used to achieve accuracy rather than a smaller number of higher order elements.

Alloy 82/182 weld passes are simulated by rings of weld metal that are deposited sequentially in layers two elements thick across the entire weld length.

The finite element model geometry of the single-J and double-J weld cases is shown in Figures 2-1 and 2-2, respectively. Each figure includes an illustration of the elements comprising the weld joints. The numbers in these elements represent the weld layers that are activated or removed as the welds are deposited and repaired.

3.3 Analysis Approach

The single-J and double-J models consist of a short length of nozzle, cladding on the inside of the nozzle, Alloy 182 buttering, stainless steel pipe, and the Alloy 82/182 weld.

For the heat transfer portion of each analysis, PLANE55 elements were used. These are four-node, 2D thermal conduction elements with a single degree of freedom (temperature) at each node. Once the transient thermal analysis was completed, these thermal conduction elements were replaced with "PLANE42" elements for the structural portion of the analysis. PLANE42 elements are four-node, 2D elements with two degrees of freedom (displacements in two directions) at each node.

Material properties were taken from Section II of the ASME Boiler and Pressure Vessel Code, 1998 Edition, to the extent provided. The high temperature yield strength and stress-strain properties of the Alloy 82/182 buttering and weld metal were taken from data provided to DEI by EdF (2). High temperature properties (e.g., at 1200ºF and higher) were estimated using data from the ASM Handbook (3), Inconel product literature (4), and research papers by Rybicki and Karlsson (5, 6). All materials were modeled as elastic-perfectly plastic so that work hardening effects are not included. Analyses were performed using typical yield strengths for the materials. The room temperature yield strengths used were as follows: stainless steel pipe (40 ksi), stainless steel cladding (51 ksi), Alloy 82/182 butter and weld (56 ksi), and low alloy steel nozzle (70 ksi).

Analyses did not include the effects of cold working due to machining or grinding of the material surfaces before or after welding. These cold worked layers are relatively thin and, while they can have a significant effect on the time to crack initiation, have little effect on crack growth.

Several structural boundary conditions were applied to the model. The nozzle end of the model (i.e., the left edge of the model as shown in Figures 2-1b and 2-2b) was fixed in the axial direction. In addition, the line of nodes at which the pipe was terminated (i.e., the right edge of the model as shown in Figures 2-1b and 2-2b) were coupled in the axial direction (constrained to have the same axial displacement) to simulate continuation of the pipe beyond the model boundary.

Additional information regarding the load steps is provided in the next section.

3.4 Loading Steps

The models were loaded in a series of steps as follows:

a. Operating Pressure and Temperature Only

Each model was first analyzed for a 2,250 psia operating pressure, a 615ºF[3] operating hot leg temperature, and combined operating pressure and temperature. The purpose of this step was to determine the operating condition stress levels without the welding residual stresses. Internal pressure loading was applied to the inside surface of the pipe (i.e., the bottom edge of the model as shown in Figures 2-1b and 2-2b). An appropriate negative pressure loading was also applied to the pipe end to simulate end reactions ("cap pressure") due to internal pressure.

b. Welding

The welding process is simulated by combined thermal and structural analyses. A transient thermal analysis is used to generate nodal temperature distributions throughout the welding process. These nodal temperatures are then used as inputs to the structural analysis that calculates resultant thermally induced stresses. The sequence of thermal analyses followed by structural analyses was duplicated for each simulated weld pass.

3 The 615ºF temperature is approximately midway between the reported 610ºF and 619ºF hot leg temperatures for VC Summer and Ringhals 4, respectively.

Heat is rapidly input to each pass of weld material at a rate that raises the peak weld metal temperature to about 3,500ºF (the heat input in the finite element model was adjusted to produce this maximum temperature) and the base metal adjacent to the weld to about 2,000ºF. After the weld heat input is stopped, the weld metal is allowed to cool—heat is conducted away by the attached pipe and nozzle—until the weld material reaches a 350ºF interpass temperature.

Cooling from the nozzle and pipe to air at an ambient temperature of 70°F by convection was modeled using a heat transfer coefficient of 5 BTU/hr-ft^2-°F, consistent with natural convection cooling in still air (convection cooling of the weld elements was not included in the model, i.e., only the dominant effects of conduction cooling of the weld metal to the pipe/nozzle base metal was simulated). To simulate the heat-sink represented by the nozzle material and pipe material far from the weld, the model edge boundaries (i.e., the left and right ends of the model as depicted in Figures 2-1b and 2-2b) were treated as 70°F heat sinks.

c. Weld Repairs

Weld repairs are simulated by deactivating elements associated with previously welded material and reapplying new weld metal in its place. Deactivation of elements essentially results in elimination of the conductive capacity or stiffness of the deactivated element in heat transfer and structural analyses, respectively.

d. Hydrostatic Testing

Components are hydrostatically tested to approximately 3,125 psi after installation. This step is included in the analysis since applied hydrostatic pressure further yields any material stressed to near yield by welding and, therefore, results in a reduction of the peak residual tensile stresses after the hydrostatic test pressure is released. In this manner, the hydrostatic testing represents a form of "mechanical stress improvement" in areas of high stress. Aside from applying pressure to all wetted inside surfaces, an axial tensile stress is applied to the end of the pipe equal to the longitudinal pressure stress in the pipe wall.

e. Operating Conditions Superimposed on Welding Residual Stresses

Operating conditions are simulated by pressurizing the inside of the model to 2,250 psi and heating all of the material uniformly to the assumed operating temperature of 615ºF. The constant operating temperature will produce thermal stresses due to the difference in coefficient of thermal expansion between the low-alloy steel nozzle, the Alloy 82/182 weld and buttering, and the stainless steel pipe. The pressure and thermal conditions are added to the model, which has already been subjected to welding (and weld repairs) and hydrostatic testing.

4
ANALYSIS RESULTS

4.1 Results for Idealized Bimetallic Pipe Weld

For perspective, a simple model of a low-alloy steel and stainless steel pipe connected by an idealized bimetallic pipe weld (i.e., a butt joint between the two materials with no weld material) was included in this study. The idealized case was analyzed under operational conditions (pressure and temperature loading) only.

A plot of the hoop (Sz) and axial (Sy) stresses in the region of the idealized bimetallic joint are shown in Figure 4-1. As anticipated, the stress distribution is consistent with the greater thermal expansion of the stainless steel pipe relative to that of the low-alloy steel (Note: the interface between the nozzle and pipe material is located at the center of each figure; the lower edge of each image is the pressurized ID surface of the pipe.)

4.2 Results for Single-J Nozzle-to-Pipe Weld

Information is limited with regard to the details of the original fabrication weld repairs at VC Summer. Consequently, three different single-J weld cases were analyzed: the as-designed weld case, an as-repaired case with ID repair weld passes made first (and OD repair welds last), and an as-repaired case with OD repair weld passes made first (and ID welds last). Each of the three single-J weld cases were analyzed using the same model geometry as described in Section 2.

Hoop and axial stress distributions in the single-J weld region under operational conditions (i.e., operational temperature and pressure loading, including the effects of the welding and hydrostatic testing that precede operation) are presented in Figures 4-2 and 4-3, respectively, for the as-designed and two repair cases. Figure 4-2 shows that ID hoop stresses are greatest for the case when OD repair welds are made first and the weld is then completed at the ID. The hoop stresses in the as-designed and ID-repaired-first cases are similar. Figure 4-3 also shows that axial stresses at the ID are higher for the repair case when the OD repair welds are made first and the weld is then completed at the ID. Comparison of the distributions in Figures 4-2 and 4-3 show that hoop stresses are higher than axial stresses for each of the three single-J cases.

Figure 4-6 illustrates two paths along which numerical stress results were extracted: 1) a path *on the inside surface of the pipe*, and 2) a path *through the centerline of the weld from the inside to the outside of the pipe*. Figures 4-7, 4-8 and 4-9 present the numerical results of the single-J weld for the as-designed, ID-repaired-first, and OD-repaired-first cases, respectively, along the two paths illustrated in Figure 4-6. Each figure shows that hoop stresses exceed axial stresses along the wetted ID surface and through the weld (from the inside to outside). Figure 4-9a shows that there is a small area at the left side of the graph where the axial and circumferential stresses on the inside surface are about the same. This is the location where a small circumferential crack was detected at VC Summer.

Select results from the three single-J weld cases are summarized in Table 4-1.

4.3 Results for Double-J Nozzle-to-Pipe Weld

Two cases were analyzed for the double-J nozzle-to-pipe weld, each using the same model (as described in Section 2): a case with ID weld passes made first (and OD repair welds last), and the case with OD repair weld passes made first (and ID welds last)

Hoop and axial stress distributions in the double-J weld region under operational conditions (welding, hydrostatic testing, temperature and pressure) are presented in Figures 4-4 and 4-5, respectively, for both (ID-first and OD-first) double-J cases. Figure 4-4 shows that the hoop stress is greatest on the side (ID versus OD) which is welded last. Consequently, ID hoop stresses are highest for the case in which the ID welds were made last. Figure 4-5 shows that axial stresses at the ID surface are comparable for both double-J weld cases, though the distributions of axial stress through the thickness (wetted inside surface to outside) differ considerably. Note that, in each stress distribution figure, the bottom edge of each image is the inside (wetted) surface and the top edge is the OD surface.

Figures 4-10 and 4-11 present the numerical results of the double-J weld for both the ID-first and OD-first cases, respectively. Again, each figure presents two graphs: hoop and axial stresses along a path *on the inside surface of the pipe* and axial and hoop stresses along a path *through the centerline of the weld from the inside to the outside of the pipe*. Each figure shows that the hoop stress exceeds the axial stress along each of the two paths considered (i.e., the wetted ID surface and through the weld centerline). However, Figure 4-10a shows that there is a region along the ID surface at which axial stress is comparable to the hoop stresses.

Select results from the two double-J weld cases are summarized in Table 4-1.

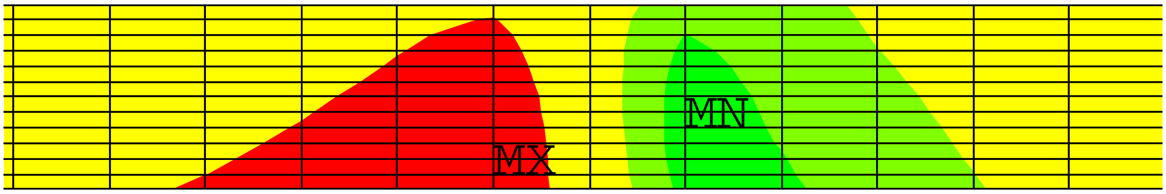

Figure 4-1a. Hoop Stress

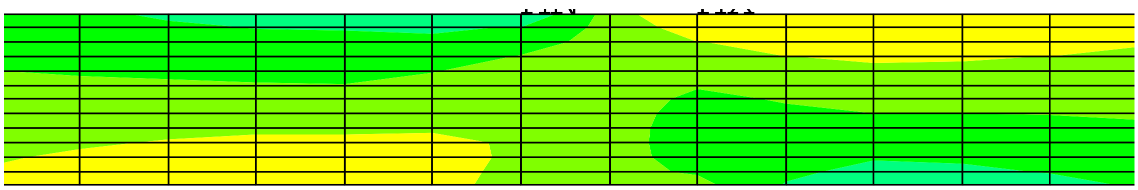

Figure 4-1b. Axial Stress

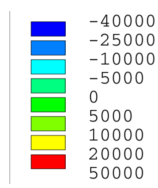

Legend – Stress Contours (ksi)

Figure 4-1
Idealized Bimetallic Weld – Operating Pressure and Temperature Only

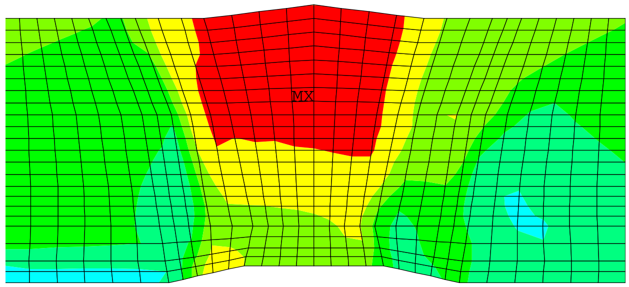

Figure 4-2a. As Designed

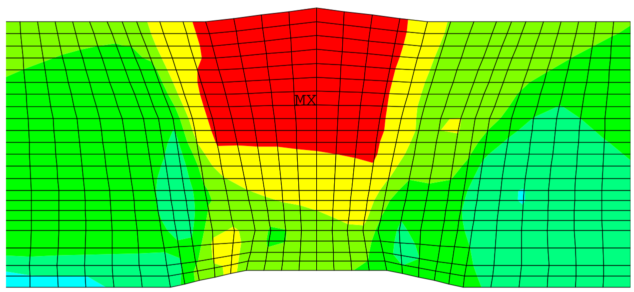

Figure 4-2b. ID Repair Weld First

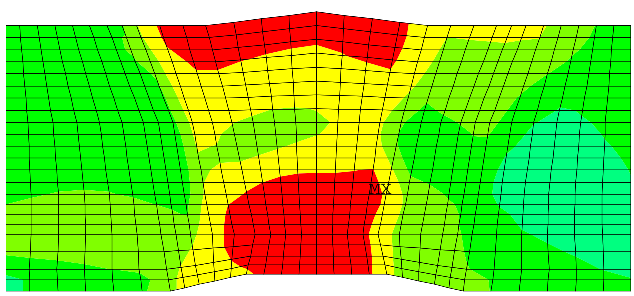

Figure 4-2c. OD Repair Weld First

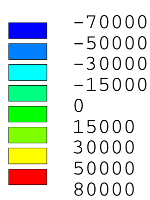

Legend – Stress Contours (ksi)

Figure 4-2
Single V-Weld – Hoop Stress (Weld Residual + Hydro Test + Operating Conditions)

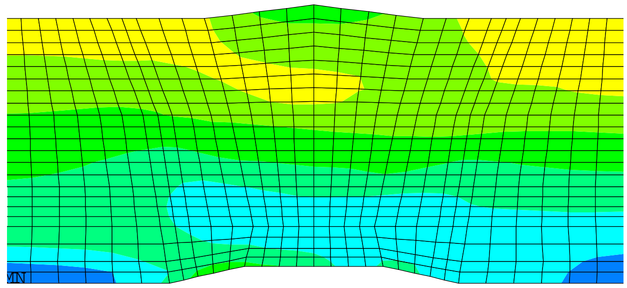

Figure 4-3a. As Designed

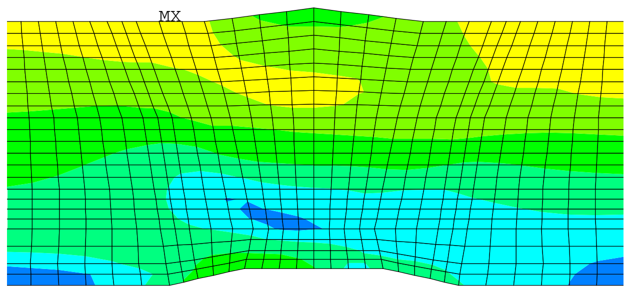

Figure 4-3b. ID Repair Weld First

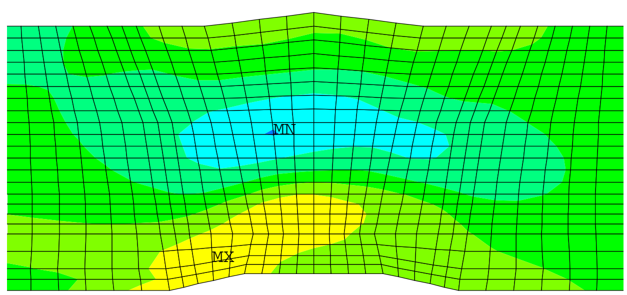

Figure 4-3c. OD Repair Weld First

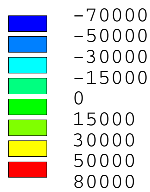

Legend – Stress Contours (ksi)

Figure 4-3
Single V-Weld – Axial Stress (Weld Residual + Hydro Test + Operating Conditions)

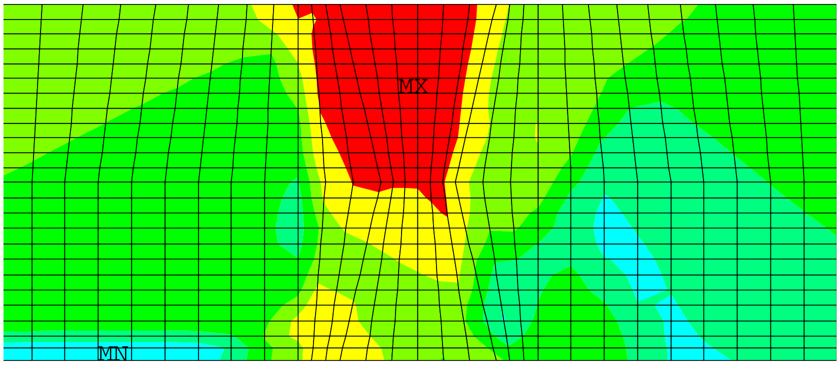

Figure 4-4a. ID Weld First

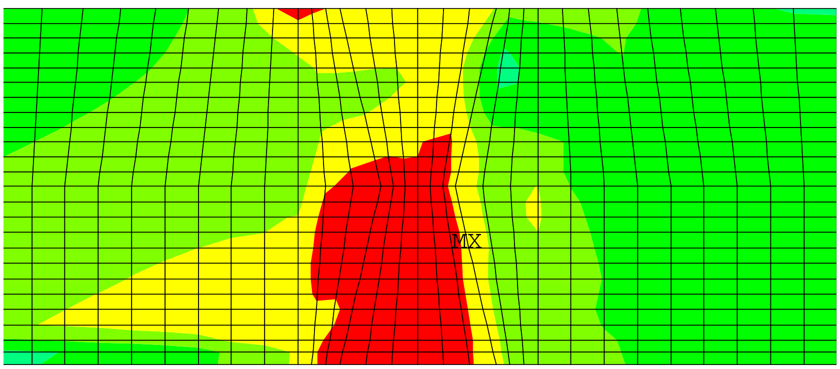

Figure 4-4b. OD Weld First

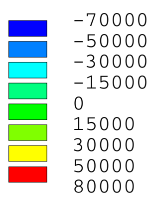

Legend – Stress Contours (ksi)

Figure 4-4
Double V-Weld – Hoop Stress (Weld Residual + Hydro Test + Operating Conditions)

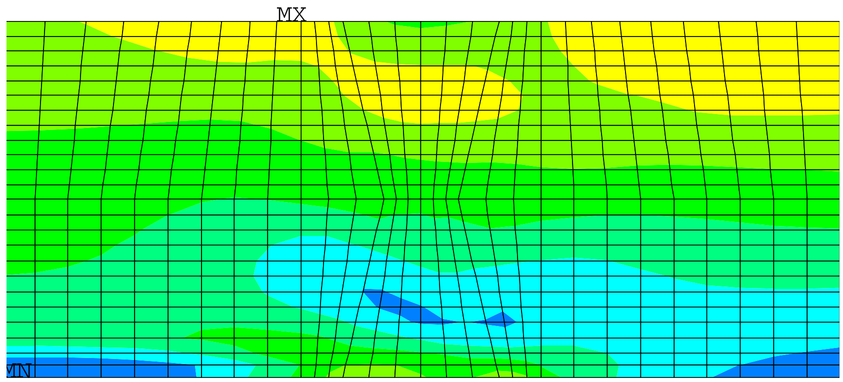

Figure 4-5a. ID Weld First

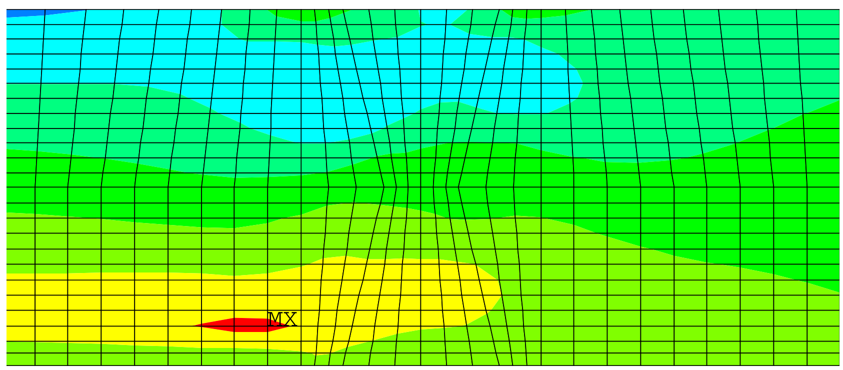

Figure 4-5b. OD Weld First

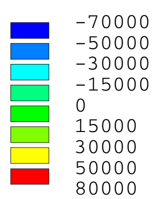

Legend – Stress Contours (ksi)

Figure 4-5
Double V-Weld – Axial Stress (Weld Residual + Hydro Test + Operating Conditions)

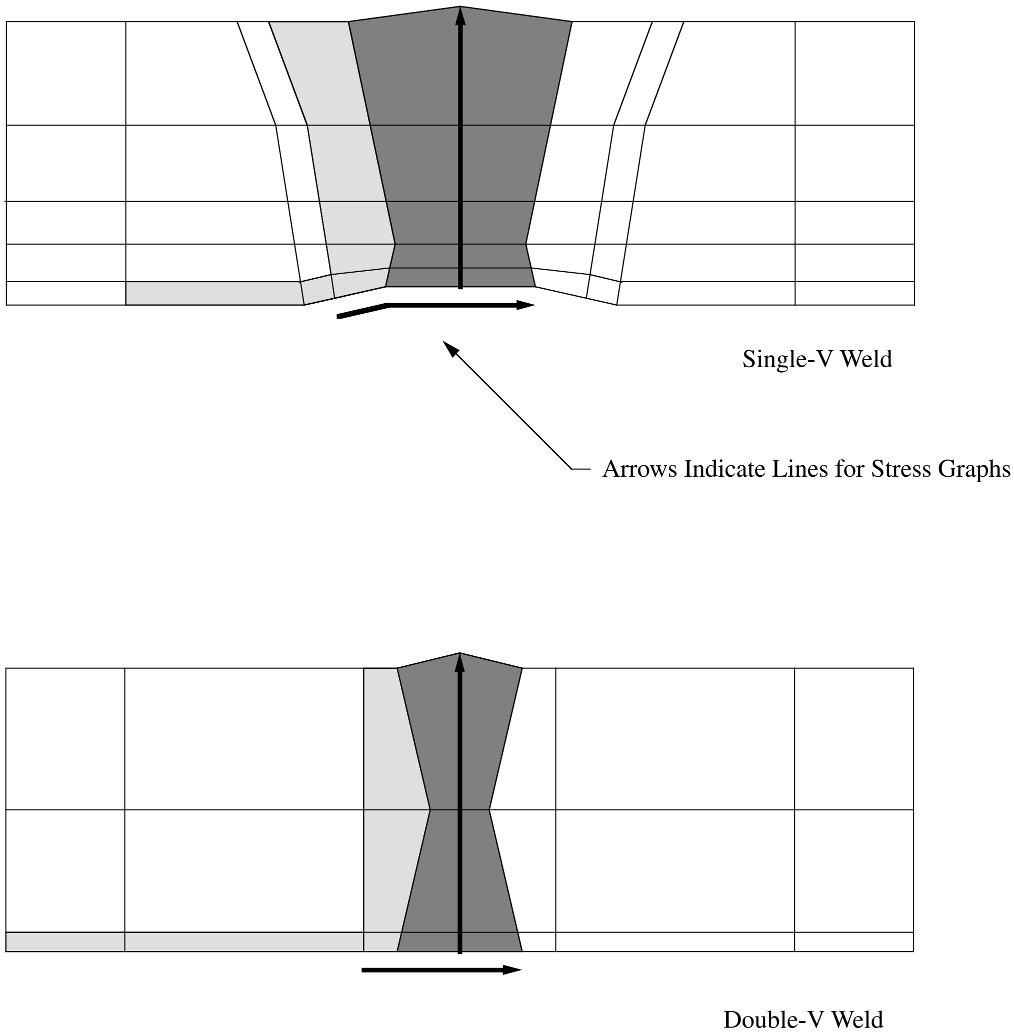

Figure 4-6
Paths For Which Results are Presented in Figures 4-7 through 4-11

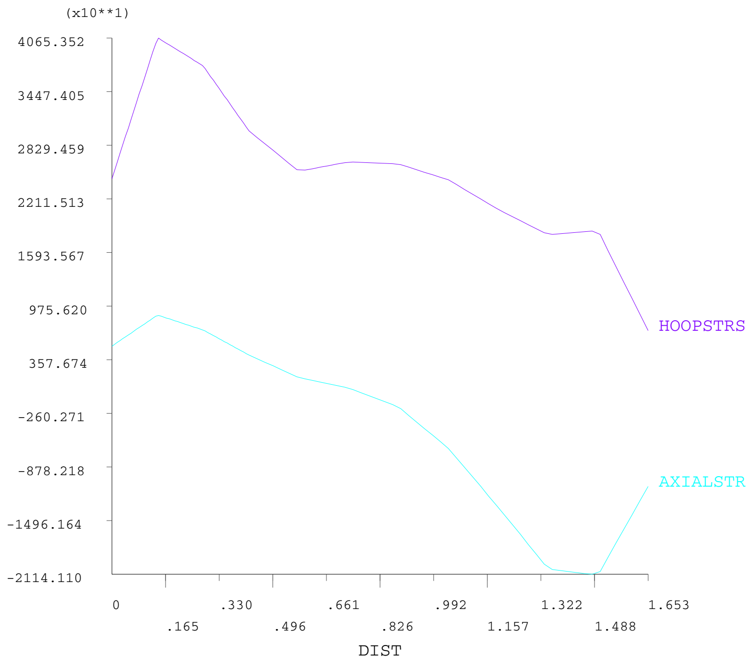

Figure 4-7a. Stresses Along Inside Surface of Weld and Buttering

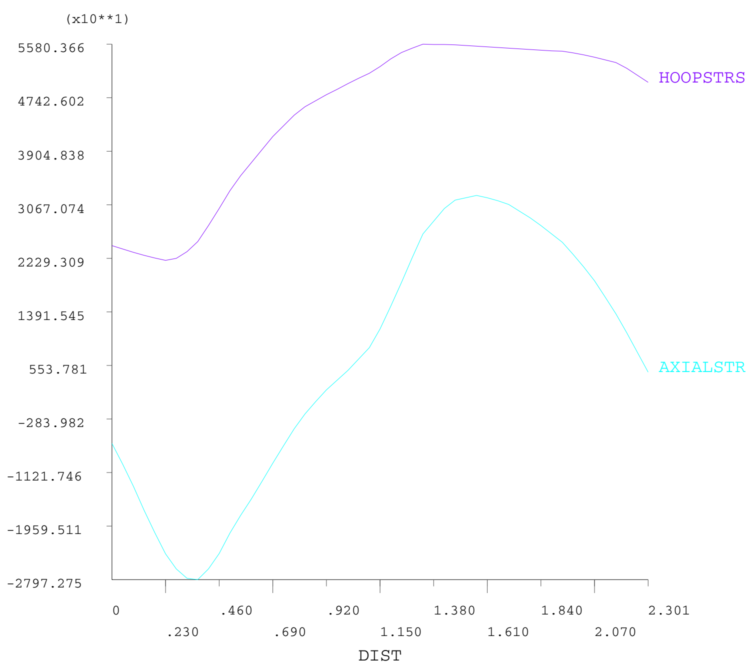

Figure 4-7b. Stresses From Inside to Outside of Pipe Through Weld Centerline

Figure 4-7
Single V-Weld – As-Designed (Weld Residual + Hydro Test + Operating Conditions)

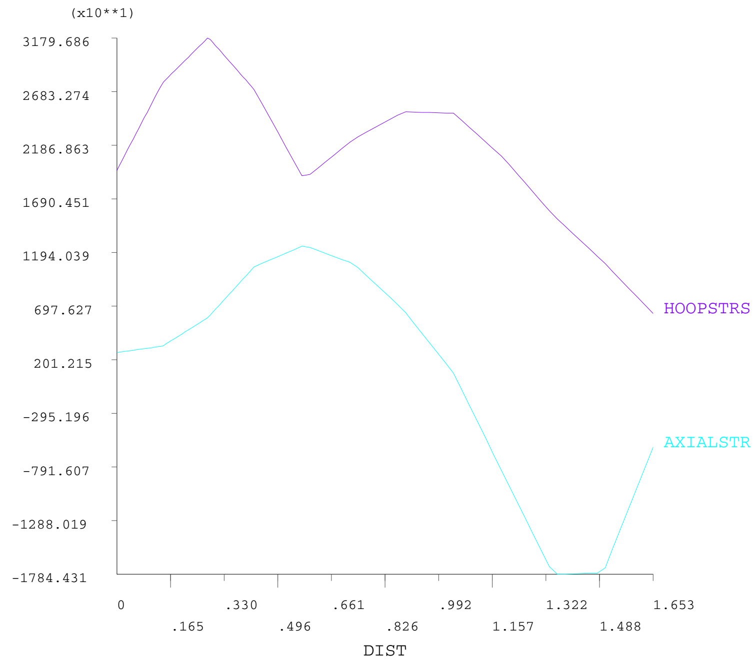

Figure 4-8a. Stresses Along Inside Surface of Weld and Buttering

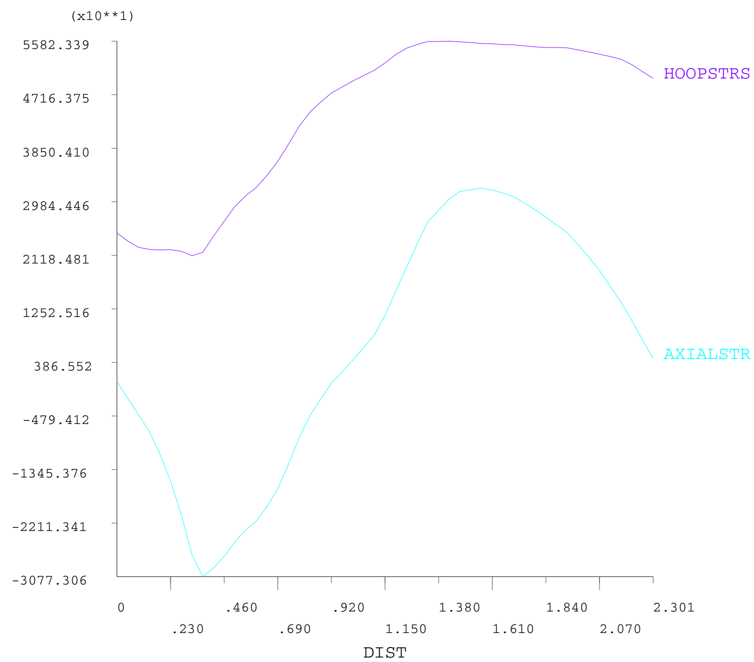

Figure 4-8b. Stresses From Inside to Outside of Pipe Through Weld Centerline

Figure 4-8
Single V-Weld – ID Repair Weld First (Weld Residual + Hydro Test + Operating Conditions)

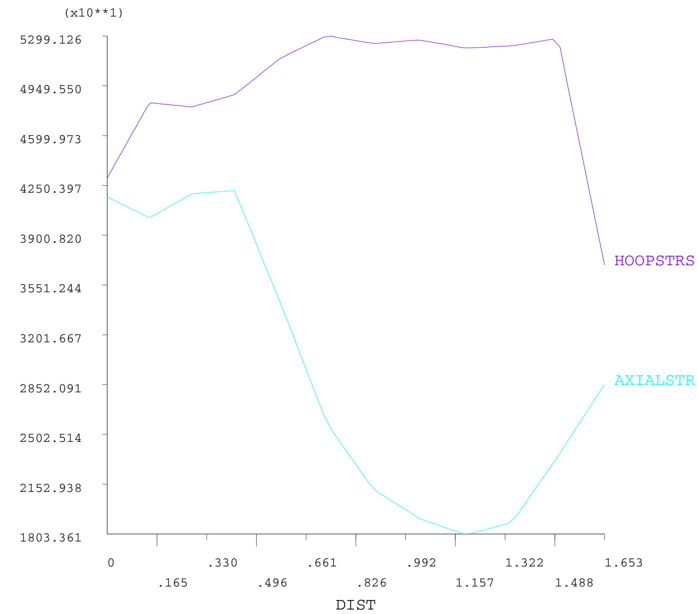

Figure 4-9a. Stresses Along Inside Surface of Weld and Buttering

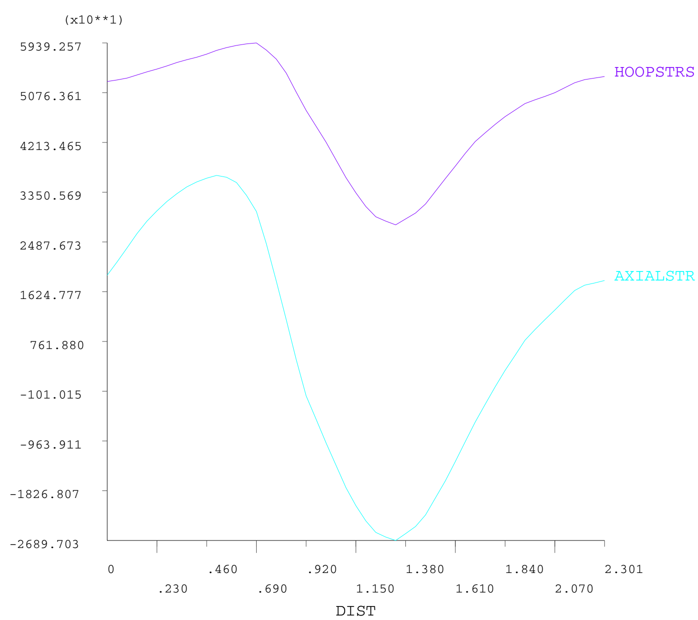

Figure 4-9b. Stresses From Inside to Outside of Pipe Through Weld Centerline

Figure 4-9
Single V-Weld – OD Repair Weld First (Weld Residual + Hydro Test + Operating Conditions)

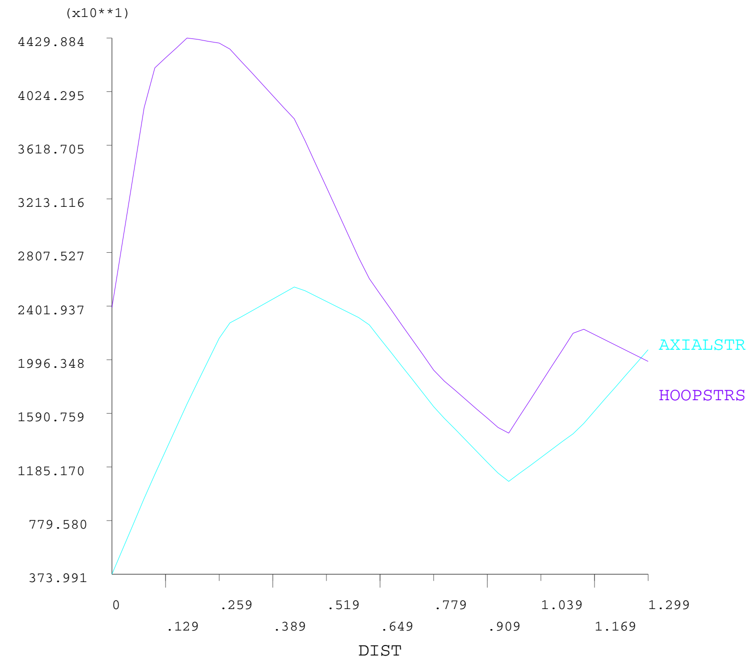

Figure 4-10a. Stresses Along Inside Surface of Weld and Buttering

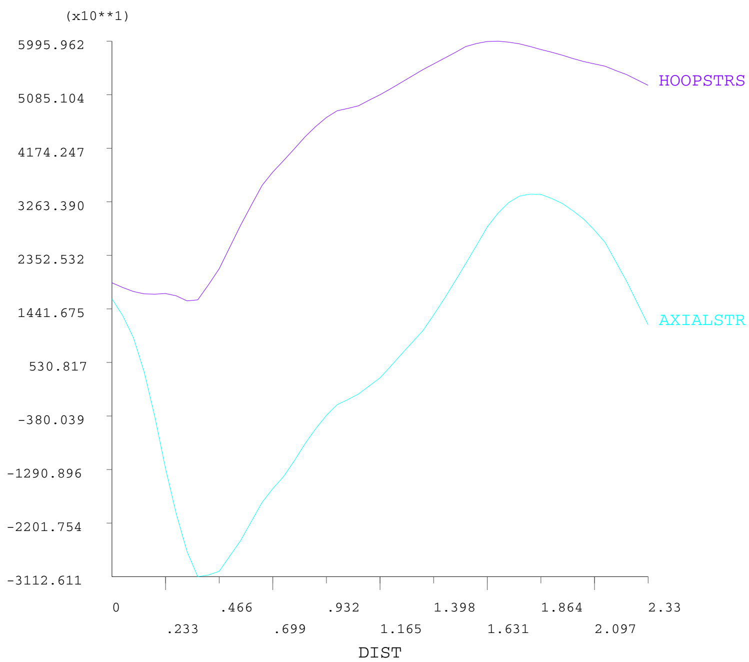

Figure 4-10b. Stresses From Inside to Outside of Pipe Through Weld Centerline

Figure 4-10
Double V-Weld – ID Weld First (Weld Residual + Hydro Test + Operating Conditions)

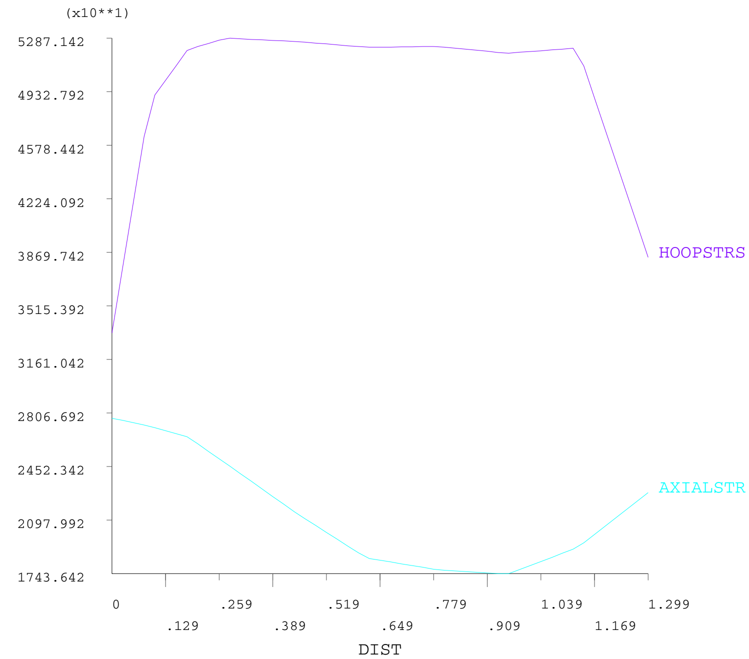

Figure 4-11a. Stresses Along Inside Surface of Weld and Buttering

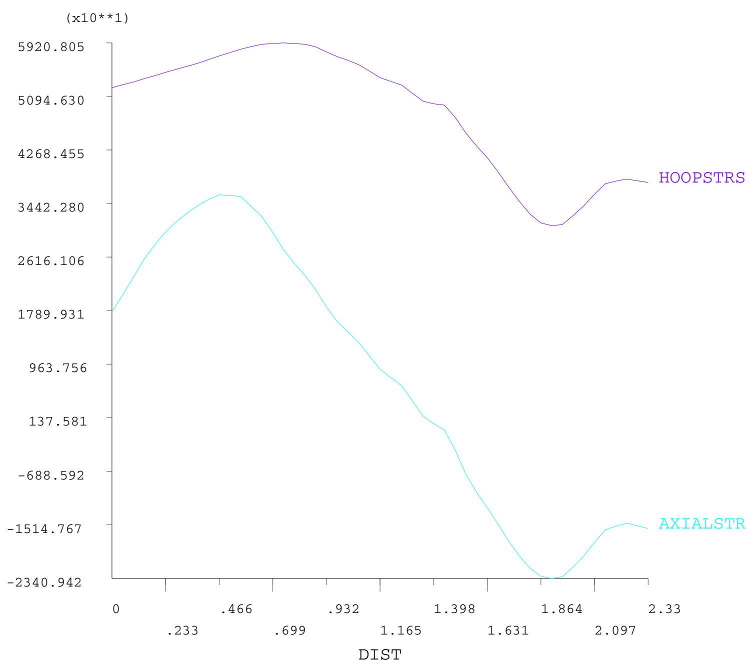

Figure 4-11b. Stresses From Inside to Outside of Pipe Through Weld Centerline

Figure 4-11
Double V-Weld – OD Weld First (Weld Residual + Hydro Test + Operating Conditions)

Table 4-1
Summary of Hot Leg Nozzle-Pipe Weld Finite Element Analysis Result

Design and Condition	Hoop Stresses (ksi)		Axial Stresses (ksi)	
	Inside Surface Operating	Mid-Wall Operating	Inside Surface Operating	Mid-Wall Operating
Single-J Welded Nozzle				
- As Designed	41	52	9	11
- As Repaired – ID Welded First	32	52	13	12
- As Repaired – OD Welded First	53	34	42	-21
Double-J Welded Nozzle				
- As Designed – ID Welded First	44	51	27	3
- As Designed – OD Welded First	53	54	28	10

All stresses include the effects of welding, hydrostatic testing, and operating conditions (pressure and temperature).

5 DISCUSSION OF ANALYSIS RESULTS

5.1 Discussion of Analysis Results

Several conclusions can be drawn from the analyses of the single-J and double-J welds.

- All cases analyzed for the both the single-J and double-J weld show that hoop stresses exceed axial stresses along the ID surface (often considerably), indicating that cracks, should they initiate at the inside surface of the welds, would be axial in orientation.
- Analyses of both the single-J weld and double-J weld configurations show that welds made first at the OD and then completed at the ID result in the higher hoop stresses along the ID surface than welds completed at the OD.
- With the exception of the as-repaired single-J case welded at the ID first, there are relatively high tensile operating condition hoop stresses of 41-53 ksi on the inside surface of the weld and buttering. Addition of new passes on the outside of the weld does not create sufficient inward deflection of the pipe to change the stress in the initial passes from tensile to compressive.
- In all cases, there are relatively high hoop stresses through the weld thickness, indicating the potential for any surface cracks to propagate in the through-thickness direction and to be axially oriented. Through-thickness axial stresses are significantly less, and often approach zero in some regions.
- There is some possibility that the cladding/buttering may have higher inside surface stresses than the welds as a result of straining material that was cold worked during machining of the weld preps. Since cold work was not modeled, this effect is not reflected in the analysis results.
- Also, the analyses are axisymmetric and there is potential for higher stresses at the ends of any partial circumferential weld repairs.

6
REFERENCES

1. Drawings showing VC Summer weld design by Duke Engineering and Services dated November 14, 2000.

2. M.H. Duc, "Specification de Calcul de Maquettes d'Adaptateurs." EdF Specification MS-92-090-A-GPE: A667M.

3. ASM Materials Handbook, Ninth Edition.

4. "Inconel Alloy 600," INCO Alloys International, Inc., Catalog Number 3M 5-85 T-7, Sixth edition, 1985.

5. E.F. Rybicki and R.B. Stonesifer, "Computation of Residual Stresses due to Multipass Welds in Piping Systems," Journal of Pressure Vessel Technology, Volume 101, May 1979, pp. 149-154.

6. L. Karlsson, et. al., "Residual Stresses and Deformations in a Welded Thin-Walled Pipe."

A
FINITE ELEMENT MODEL AND RESULTS—SINGLE-J WELD AS-DESIGNED CONFIGURATION

This appendix presents the finite element analysis results after each load step is applied to illustrate the independent effects of each nozzle loading step. The case presented is the as-designed single-J weld configuration. Results provided for each step are the hoop stress and axial stress distributions in the weld region.

Results are provided for the following load steps and load combinations.

- Welding residual stresses (Figure A-1)
- Peak stresses during hydrostatic testing (Figure A-2)
- Stresses after hydrostatic testing (Figure A-3)
- Pressure only (Figure A-4)
- Temperature only (Figure A-5)
- Pressure and temperature (Figure A-6)
- Operating conditions (weld residual stresses + stresses due to hydrostatic testing + stresses induced by temperature and pressure) (Figure A-7)

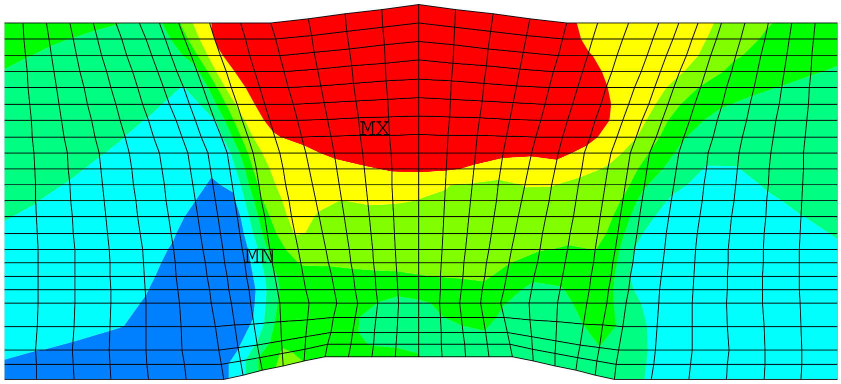

Figure A-1a. Hoop Stress

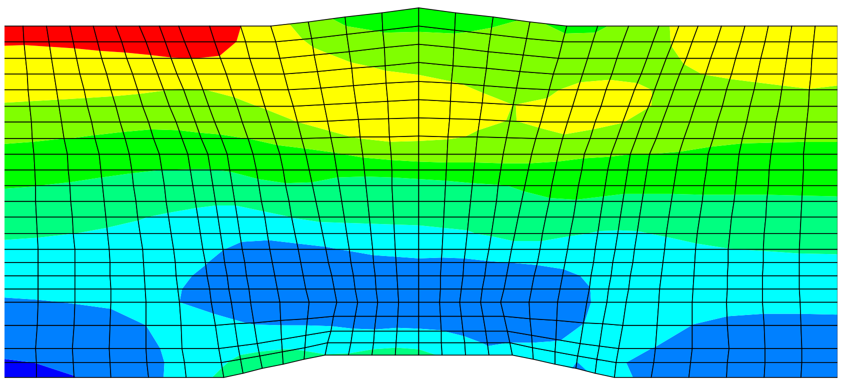

Figure A-1b. Axial Stress

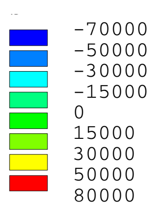

Legend – Stress Contours (ksi)

Figure A-1
Single-J Weld – Weld Residual Stress Distributions

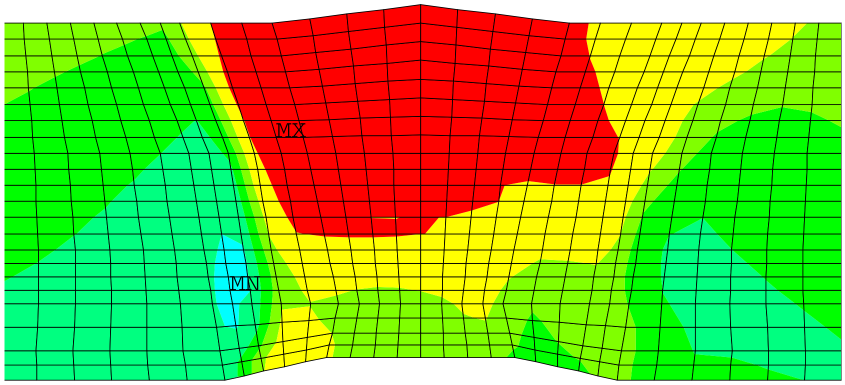

Figure A-2a. Hoop Stress

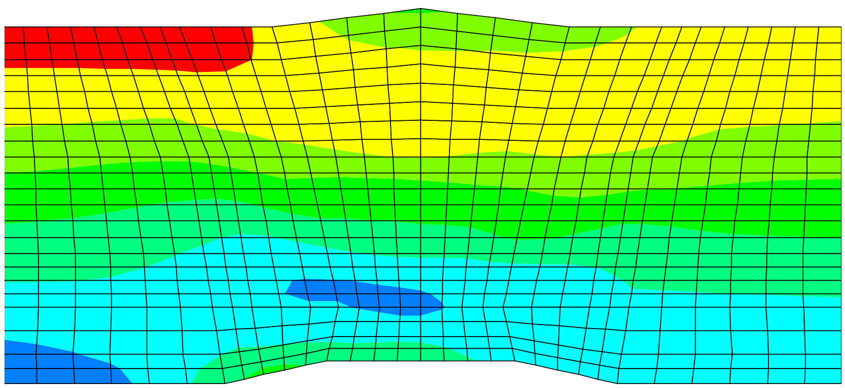

Figure A-2b. Axial Stress

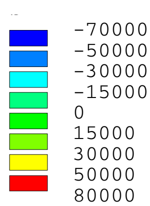

Legend – Stress Contours (ksi)

Figure A-2
Single-J Weld – Peak Hydro Test Stress Distributions

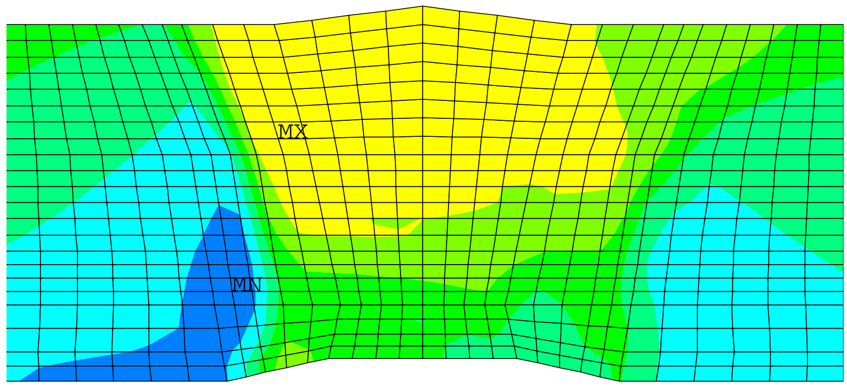

Figure A-3a. Hoop Stress

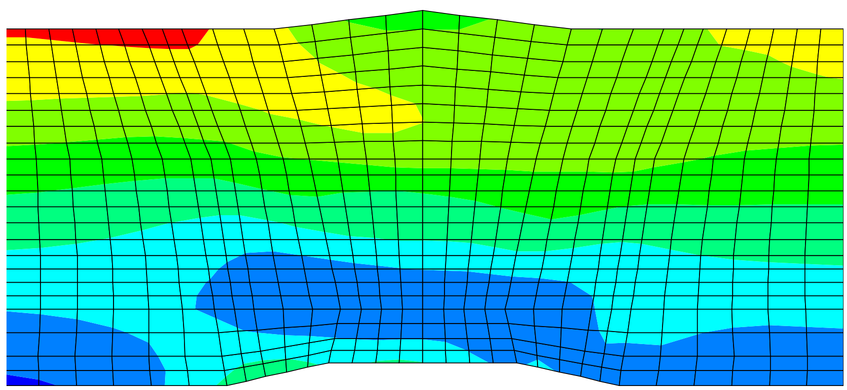

Figure A-3b. Axial Stress

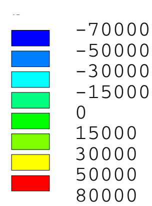

Legend – Stress Contours (ksi)

Figure A-3
Single-J Weld – Stress Distributions After Hydro Test

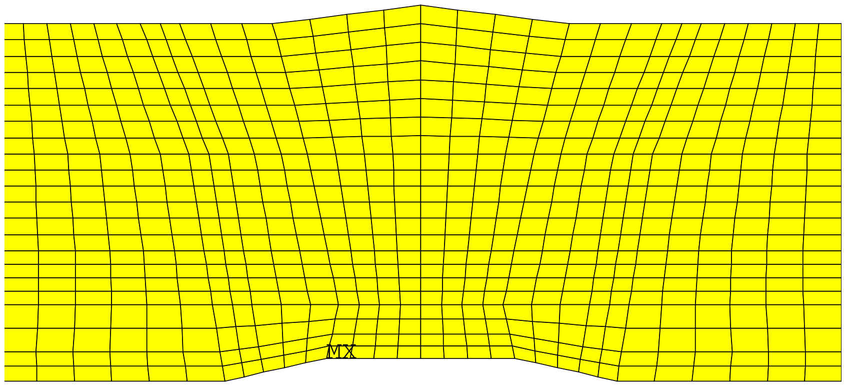

Figure A-4a. Hoop Stress

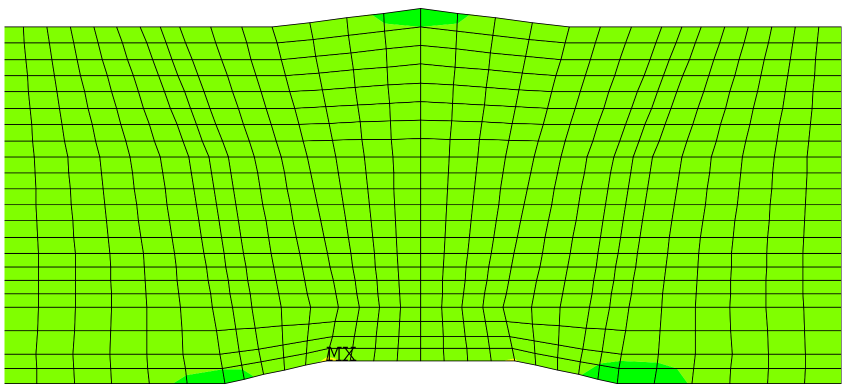

Figure A-4b. Axial Stress

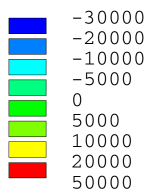

Legend – Stress Contours (ksi)

Figure A-4
Single-J Weld – Stress Distributions due to Operating Pressure Only

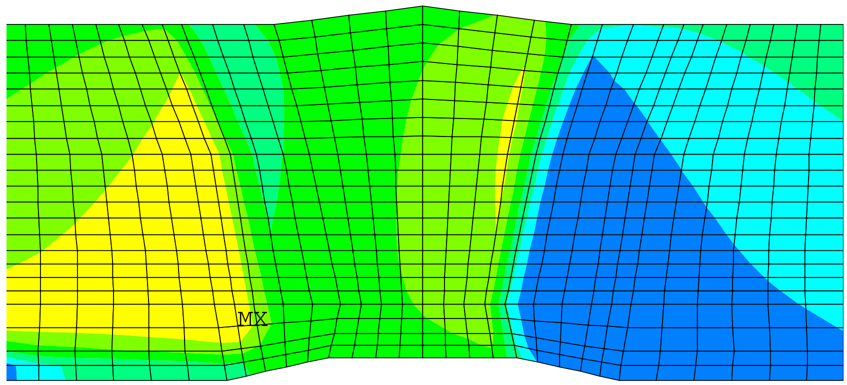

Figure A-5a. Hoop Stress

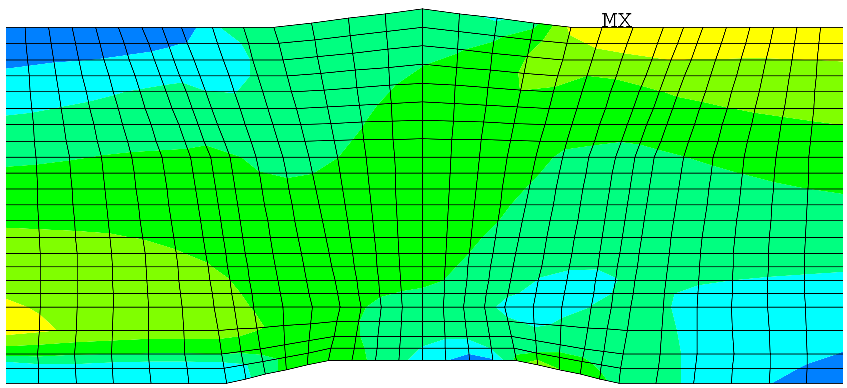

Figure A-5b. Axial Stress

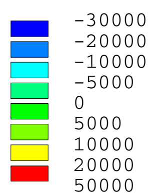

Legend – Stress Contours (ksi)

Figure A-5
Single-J Weld – Stress Distributions due to Operating Temperature Only

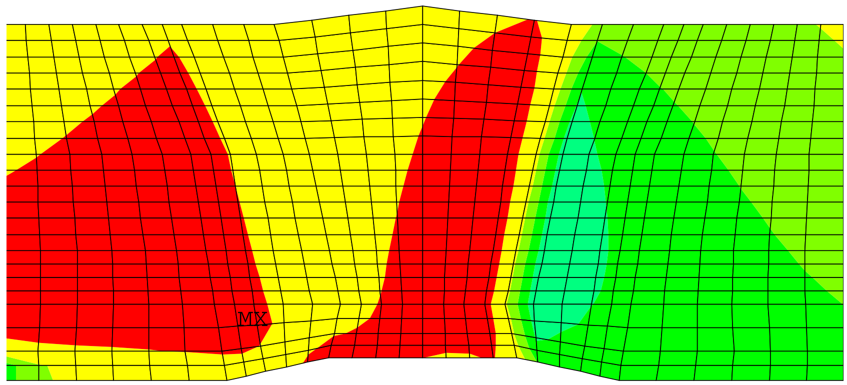

Figure A-6a. Hoop Stress

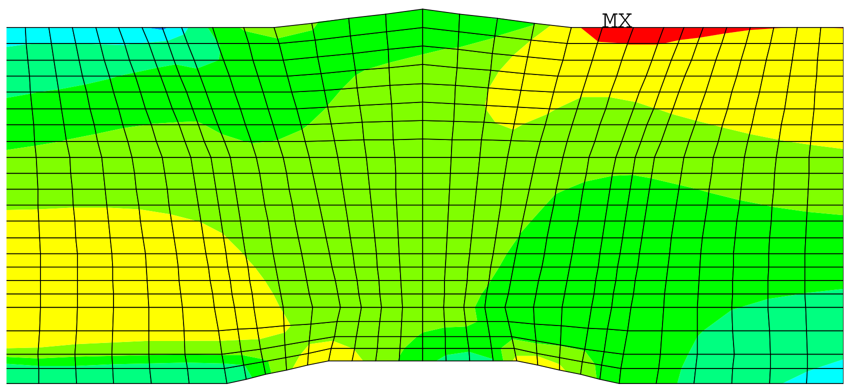

Figure A-6b. Axial Stress

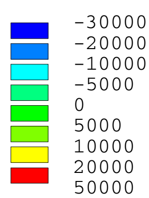

Legend – Stress Contours (ksi)

Figure A-6
Single-J Weld – Stress Distributions due to Operating Pressure and Temperature

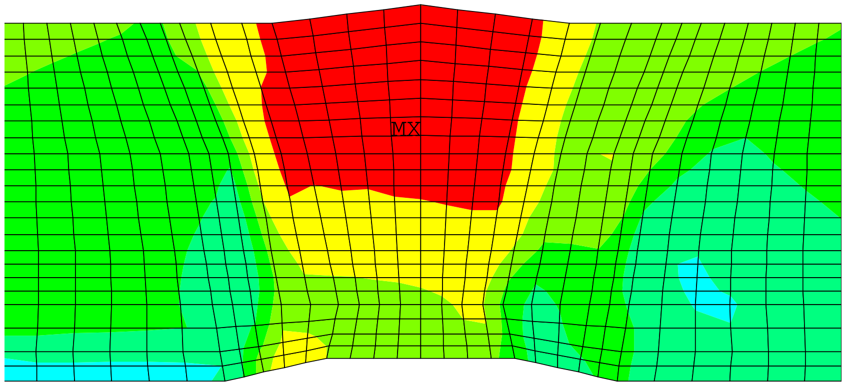

Figure A-7a. Hoop Stress

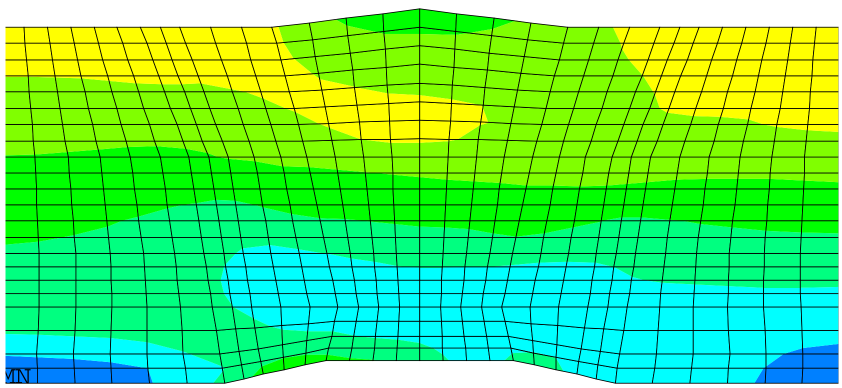

Figure A-7b. Axial Stress

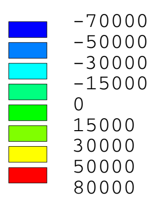

Legend – Stress Contours (ksi)

Figure A-7
Single V-Weld – Stress Distributions (Weld Residual + Hydro Test + Operating Conditions)

Targets:
Materials Reliability Program
Nuclear

About EPRI

EPRI creates science and technology solutions for the global energy and energy services industry. U.S. electric utilities established the Electric Power Research Institute in 1973 as a nonprofit research consortium for the benefit of utility members, their customers, and society. Now known simply as EPRI, the company provides a wide range of innovative products and services to more than 1000 energy-related organizations in 40 countries. EPRI's multidisciplinary team of scientists and engineers draws on a worldwide network of technical and business expertise to help solve today's toughest energy and environmental problems.

EPRI. Electrify the World

Printed on recycled paper in the United States of America

1001501

EPRI • 3412 Hillview Avenue, Palo Alto, California 94304 • PO Box 10412, Palo Alto, California 94303 • USA
800.313.3774 • 650.855.2121 • askepri@epri.com • www.epri.com